

Automatic defect depth estimation for ultrasonic testing in carbon fiber reinforced composites using deep learning

Xiaoying Cheng^{a,b}, Gaoshen Ma^a, Zhenyu Wu^{a,b,*}, Hongfei Zu^a, Xudong Hu^a

^a Key Laboratory of Modern Textile Machinery Technology of Zhejiang Province, Zhejiang Sci-Tech University, Hangzhou, 310017, China

^b Zhejiang Provincial Innovation Center of Textile Technology, Zhejiang Sci-Tech University, Hangzhou, 310017, China



ARTICLE INFO

Keywords:

Ultrasonic testing
Carbon fiber reinforced composite
Automatic ultrasonic signal classification
LSTM

ABSTRACT

Ultrasonic testing (UT) is commonly used to inspect the geometric shape of internal damage in composite materials and the test results need to be interpreted by trained experts. In this work, an automatic signal classification method based on deep learning is proposed for depth estimation of the defects introduced by low-velocity impact (LVI) in carbon fiber reinforced plastics (CFRPs). Three kinds of neural networks, LSTM, CNN, and CNN-LSTM are used to analyze the attributes with different depths. Then, trained models are applied to identify the depth information of impact damage. The results show that the CNN-LSTM model is a more accurate in-depth classification for LVI defects in CFRP based on A-scan signals than the other two structures.

1. Introduction

Carbon fiber reinforced plastic (CFRP) is widely employed in the fields of aerospace, wind energy, and automotive industry, etc. due to its high specific modulus and strength, and excellent fatigue resistance properties [1]. Although they have these advantages, CFRPs are also prone to contain defects caused by the manufacturing process and damage caused by low-velocity impact (LVI) [2,3]. Moreover, these defects and damages, such as matrix crack, debonding, and delamination, are barely visible and could develop into more severe states during normal operation and dramatically reduce residual strength. Therefore, it is crucial to regularly evaluate the internal state of CFRPs to prevent catastrophic failures.

Various non-destructive testing (NDT) techniques have been developed to quantitatively evaluate the state of internal defects of materials without compromising their structural integrity. However, the task of NDT for composites is more complicated because of the complex damage phenomena and the anisotropy of reinforcement structures. The commonly used NDT methods for CFRPs include ultrasonic testing (UT) [3], infrared thermography (IR) [4], X-ray tomography (CT) [5], and acoustic emission (AE) [6], etc.

As an easy-to-use and portable NDT method, UT is increasingly used in the damage evaluation of composite materials. Moreover, the pulse-echo modality, which utilizes the echo amplitude and flight time to determine the existence and location of defects, is widely applied for

internal flaw detection of CFRPs [3,7]. Aymerich and Meili used the TOF method to characterize CFRP impact delamination damage layer by layer to obtain the extension and thickness position of delamination damage [8]. In addition, Morokov et al. used high-resolution imaging based on the TOF method to achieve damage distribution at different lamination positions [9].

To further obtain the spatial distribution of damage, Hauffe et al. and Sadeghi et al. utilized morphological processing to extract and optimize the contour of the damage detection image to obtain a more accurate damage area [10,11]. Yang et al. used a method based on the combination of TOF and an optical microscope to characterize the impact delamination defect space layer by layer [12]. Wang et al. and Angelika et al. reconstructed the damage state in three dimensions according to the ultrasonic signal [13,14]. Although those methods are effective in detecting very complex structures [15], they require a lot of prior knowledge that depends on the subjective analysis of experienced testers, which may compromise the reliability of the test result interpretation [3]. Therefore, To minimize the error caused by human factors, the automatic defect detection method has attracted much attention recently to simplify the procedure and improve detection efficiency [16].

More and more researchers have implemented automated ultrasonic inspection methods based on deep learning (DL) frameworks. For example, Miorelli et al. utilized convolutional neural networks (CNN) to estimate the information about the localization and size of defects in the

* Corresponding author. Key Laboratory of Modern Textile Machinery Technology of Zhejiang Province, Zhejiang Sci-Tech University, Hangzhou, 310017, China.
E-mail address: zistwuzhenyu@163.com (Z. Wu).

aluminum plate [17]. To improve the generalization ability and robustness of the automated ultrasonic detection method, deep learning (DL) frameworks are introduced for the interpretation of inspection results [18,19]. However, when the defects are located at adjacent depth positions, the ultrasonic detection signals of the defects are extremely similar and cannot be accurately distinguished. To improve the accuracy of defect identification, Guo et al. and Gao et al. performed the high-precision classification (with an improved softmax classifier) of similar signals of known defects in adjacent depths, which were produced artificially via inserting foreign objects and drilling holes [20,21].

The above works show that the DL framework can realize defect identification in ultrasonic inspection with high classification accuracy even when the defect signals are extremely similar. In those studies, artificial defects, such as drilled dents and pre-embedded films, are prevalent since the known defect information is necessary for the neural network training process. However, to our best knowledge, there are few studies have validated the effectiveness of the DL networks trained by artificially prefabricated defects on the unknown damage in the CFRP, which is generated during normal service.

Therefore, this work focuses on the identification of defects at unknown depth locations in CFRPs. Firstly, CFRP plates with artificial defects and low-velocity impacted (LVI) damage are prepared and scanned by ultrasonic equipment. Then a DL framework based on CNN-LSTM is proposed and trained by A-scan results from artificial defects. At last, the trained proposed network is used to estimate the unknown damage state inside the impacted sample, and the classification performance is validated by comparing it with the testing results of other networks.

2. Experimental methods and models

2.1. Sample preparation and methods

Two kinds of CF prepgres were used in this work: unidirectional (UD) fabrics and plain woven (PW) fabrics. Two layers of PW fabrics were placed on both surfaces to cover 20 layers of UD fabrics, which were in order $[0/90]_{5s}$ (Fig. 1). The purpose of adding PW fabrics is improving the detectability of damage and reduce the uneven surface caused by non-crumped fabrics inside [22], which in turn affects the results of ultrasonic nondestructive testing. The thicknesses of PW and UD fabrics are 0.32mm and 0.20mm, respectively, and the total thickness of the

composite plates, which were fabricated via Autoclave Process technology, were controlled within 4 ± 0.1 mm.

Two types of samples were prepared for experiments: an artificial defect sample and LVI damage samples. The dimension of the artificial defect sample is 200mm × 70mm, as shown in Fig. 1a. Since there are total of 22 layers of CF fabrics, 23 dents with 6 mm diameter and different depths were drilled on one side of the sample. The first dent was 0.16 mm and then the depth of each dent progressively increased by 0.16 mm–3.84 mm at last. The purpose of the specific depth setting was to prepare for the ultrasonic scanning process to obtain A-scan data of delamination damage between each pair of adjacent layers. In Section 3, the data was used for the network training. The other samples were prepared for LVI tests according to the ASTM D7136. As shown in Fig. 1b, the samples were cut into the size of 150mm × 100mm.

The LVI tests were based on the ASTM D7136 standard. The impacting head is in hemispherical shape with a 16 mm diameter and the total mass of the impactor is 3.416 kg. A dedicated clamp was used to fix the sample during the LVI test. A series of LVI tests with different impact energies were performed on the samples as shown in Table 1. The LVI experiments are performed on three different plates with 5 J energy as the initial level and 2.5 J energy increments thereafter.

Olympus Omniscan-MX2 was used for defect detection of CFRP plates. A 5 MHz center frequency linear phased array probe (5L64-L1) and a wedge (SL1-0L-WHC) were used and the scanning position was acquired through the encoder (ENC1-2.5-DE). The C-scan, B-scan and S-scan results were used to evaluate the damage inside the sample and A-scan data were input into the networks for training and testing (Fig. 2). The number of A-scan signal points in the echogram was 320. Before the ultrasonic scanning test, the velocity of the sound in CFRP was calculated according to the time of flight and the average value is 2750 m/s for the samples in this work.

Table 1
The key parameters of the LVI tests.

Name	Impact height	Impact energy	Velocity
CFRP-1	0.15 m	5J	1.71 m/s
CFRP-2	0.22 m	7.5J	2.07 m/s
CFRP-3	0.30 m	10J	4.20 m/s

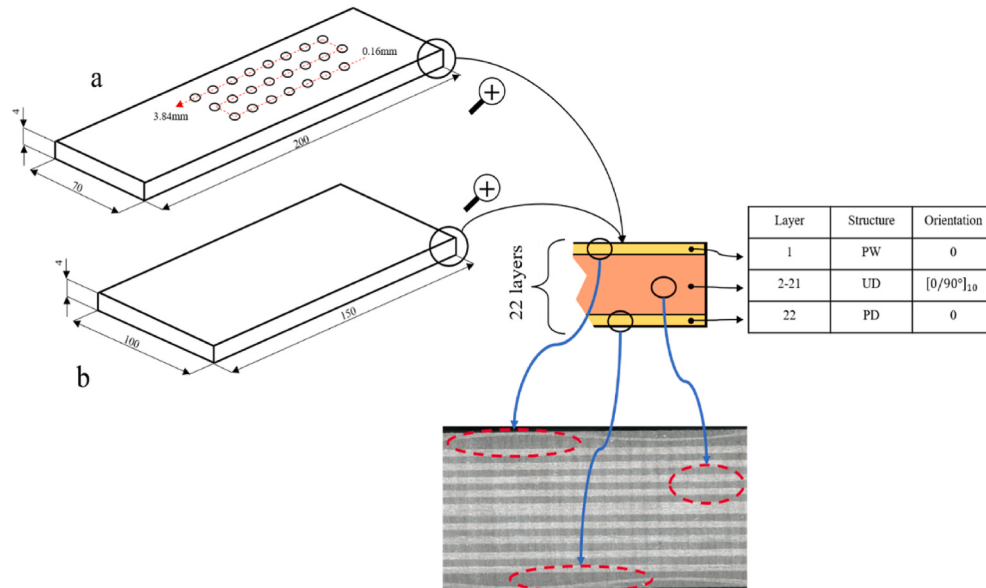


Fig. 1. The structure of CFRP samples: a) the sample with artificial dent; b) the sample for LVI tests.

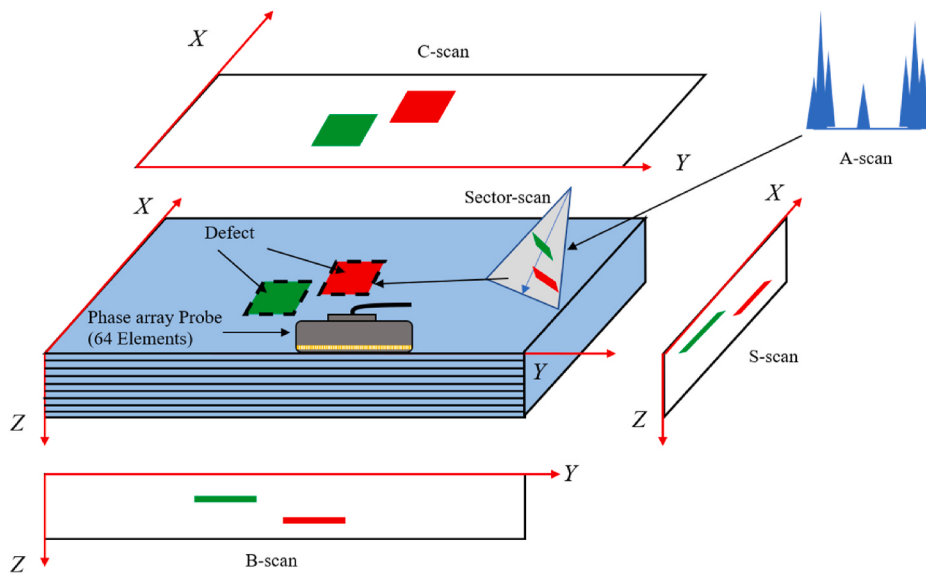


Fig. 2. The illustration of a typical ultrasonic testing mode.

2.2. Deep learning model

In this work, inspired by the paper [23], CNN-LSTM was built, as shown in Fig. 3, and a simple three-layer LSTM [24] and a simple four-layer CNN [25] neural network were built for comparison.

BiLSTM is a bidirectional time memory unit that can capture the key information of the input quantity. Many of its internal gating units can decide to discard part of the information to update the weights of the neural network unit, the forgetting gate determines part of the information in the united states, the inputs decide to update the unit state information, and the outputs filter the output according to the unit state. The bidirectional LSTM network propagation mechanism is shown in Fig. 4a, the basic composition unit structure is shown in Fig. 4b, and the calculation method of gating is shown below. Convolution kernel (Conv) and maximum pooling layer (Maxpool) are mainly used for feature extraction and data dimensionality reduction to speed up the calculation of the model. Batch normalization (BN) enables the output of the neural network layer to be adjusted with a small batch of parameters during the training process of the model, making the data more stable. The Fully connection layer (FC) converts the calculated data of the model to the tag space of the sample and then inputs the data to the softmax layer. Finally, softmax converts the obtained data into a probability function to determine the final output result.

$$i_t = \sigma(W_i \cdot [h_{t-1}, x_t] + b_i) \quad (1)$$

$$f_t = \sigma(W_f \cdot [h_{t-1}, x_t] + b_f) \quad (2)$$

$$o_t = \sigma(W_o \cdot [h_{t-1}, x_t] + b_o) \quad (3)$$

$$\tilde{C}_t = \tanh(W_C \cdot [h_{t-1}, x_t] + b_C) \quad (4)$$

$$C_t = f_t * C_{t-1} + i_t * \tilde{C}_t \quad (5)$$

$$h_t = o_t * \tanh(C_t) \quad (6)$$

The performances of all the models were measured by four evaluation indicators: Accuracy, Precision, Recall, and F1. Accuracy (ACC) is the ratio of the number of correctly classified samples to the overall samples. Precision (PRE) is the ratio of the number of correctly predicted samples to the sum of the number of correctly predicted samples of a category and the number of other samples incorrectly predicted as the number of samples of this category. Recall (REC) is the ratio of the number of correctly predicted samples of a category to the sum of the number of correctly predicted samples of a category and the number of samples of this category incorrectly classified as the number of samples of other categories. F1 is the harmonic average of ACC and REC, the larger the value, the better the robustness of the neural network.

$$ACC = \frac{TP + TN}{TP + FN + TN + FN}, \quad (7)$$

$$PRE = \frac{TP}{TP + FP}, \quad (8)$$

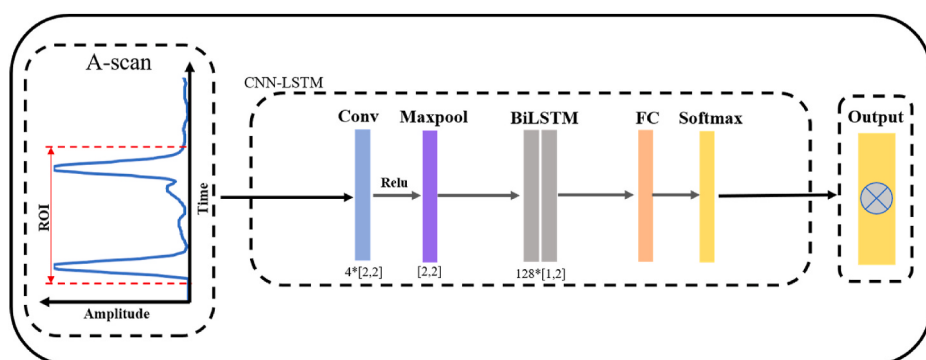


Fig. 3. Schematic diagram of the neural network model.

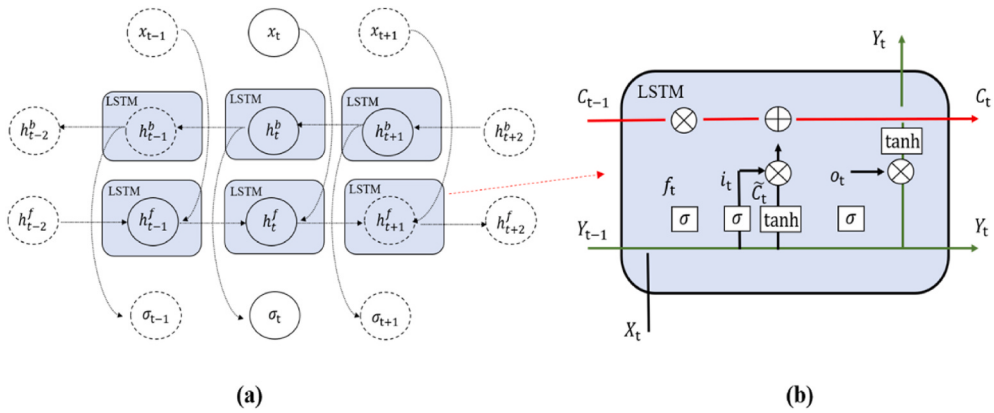


Fig. 4. The Bi-LSTM model: a) Bi-LSTM network model, b) Basic composition unit.

$$REC = \frac{TP}{TP + FN},$$

$$(9) \quad F1 = \frac{2TP}{2TP + FP + FN}, \quad (10)$$

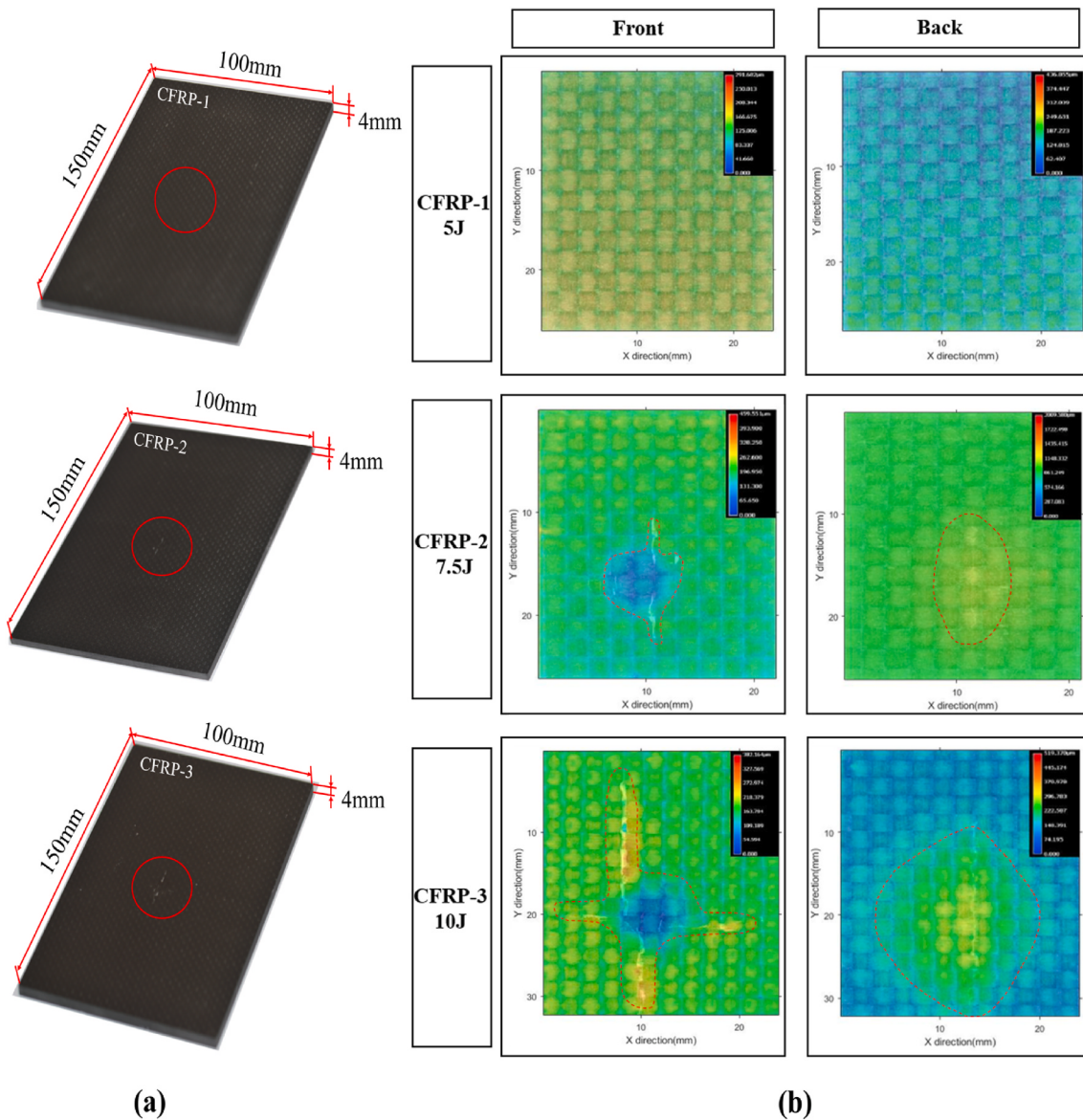


Fig. 5. Optical results of laminates after impacted at different energy levels, a), optical image, b), depth of field.

where true positive (TP) refers to the number of samples correctly predicted by the predicted category and the real category. False negative (FN) refers to the number of samples classified into other categories. False positive (FP) refers to the number of samples of other categories wrongly divided into prediction categories. True negative (TN) refers to correctly predicting the number of samples of other categories into the number of samples of other categories.

3. Results and comparison

3.1. Low velocity impact testing

After the LVI tests were performed, the impacting damage of all samples was observed by the depth of field (3D optical image mosaic) via an optical microscope (VHX-7000). As shown in Fig. 5, there is no obvious damage on the front and back surface of the sample impacted at the 5J level, and there is no height difference on both sides. For the sample impacted at 7.5J level, there are post-impact indentation and short cracks on its front surface, and slight protrusion can also be measured on the back side, which indicated that possible delamination damage had occurred in that area. When the impact energy reached the 10J level, the cross-shaped crack was observed clearly on the impacted surface and the protrusion on the back side is also much larger than that from the CFRP-2 sample.

The ultrasonic results of the artificially defected sample and CFRPs after impact are shown in Figs. 5 and 6, respectively. It is worth mentioning that, the detection results are not clear for the near-surface artificial defect, i.e., 0.16 mm and 3.68 mm delamination in Fig. 6a. With the help of the morphological processing method, the defect shapes are more distinguishable in the boundary as shown in Fig. 6b, where the echo of the defect at 0.16 mm is covered by the initial echo and that of the defect at 3.68 mm is weakened due to acoustic attenuation and buried in ambient noise [3]. The reverberation artifacts produced by the presence of the bottom hole are shown in the red dashed line in Fig. 6c, which are caused by the repetitive echoes generated by the ultrasonic

waves bouncing between the medium and the boundary of the samples [2]. Therefore, only the region of interest is intercepted for the following analysis to eliminate the effect of the artifacts. Fig. 6d shows the S-scan information of the CFRP-3 specimen after the low-velocity impact test. The damage extends along the red arrow direction, which is consistent with the cone damage morphology described in Ref. [14].

Fig. 7 illustrates the ultrasonic C-scan and D-scan (the stereoscopic display of reflectors in the test target) of CFRPs after the LVI test. According to the depth of field diagram and ultrasonic testing results mentioned above, CFRP-1 is free of defects after the impact test, and CFRP-2 has fewer A-scan signals. In the next section, seven defects (CFRP-3) with strong echo (labeled in CFRP-3) were selected for the validation of the trained networks. The depth information of each damaged region read by ultrasonic D-scan is shown in Fig. 7b.

3.2. Deep learning method

A dataset based on 2694 ultrasonic A-scan signals from the sample with artificial dent was used for network training. According to Ref. [24], the data was divided into two groups, 70% data for the training set (30% of which was used for validation) and 30% data for the testing set, as shown in Table 2. To eliminate the disturbance of reverberation artifacts on the network training, only the first 187 data from each A-scan signal, which covered the thickness of the samples, The schematic diagram of ultrasonic signals of different defects were shown in Fig. 8. Another dataset consisted of the A-scan signals of the labeled damaged areas from the impacted CFRP-3 sample (as shown in Fig. 7a) and was used for the validation of the trained networks.

The evaluation indexes of each neural network model were listed in Table 3, and all the ACC were above 0.9. The performance of each model was measured by the F1 score, and the CNN model had the best performance, followed by the CNN-LSTM. The evaluation indexes of CNN-LSTM were always better than LSTM. In terms of running time, the running time of LSTM is 144 s, and the running time of CNN is 18 s. Due to the use of the convolution layer (feature extraction), the running time

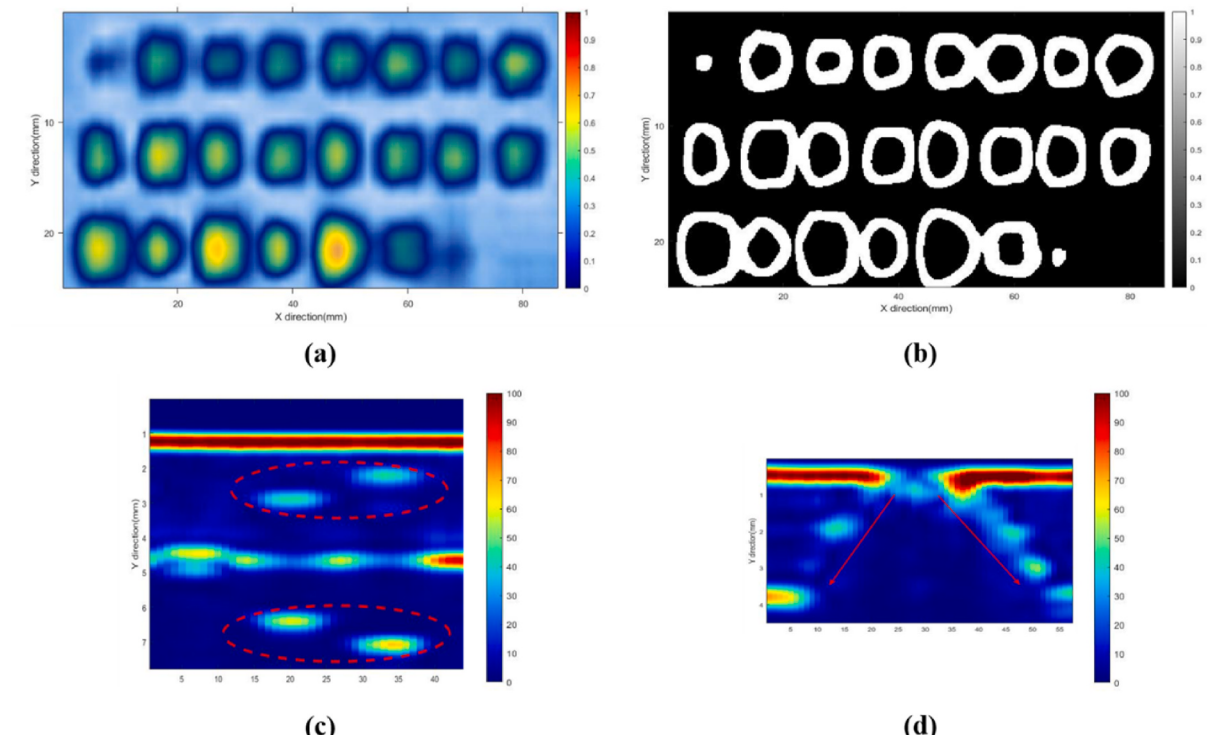


Fig. 6. Ultrasonic testing of artificial prefabricated defective plates: a) the ultrasonic C-scan image of the artificial defects, b) the ultrasonic C-scan binary image, c) the artifact image of the artificial defects, d) the ultrasonic S-scan image of the impacted sample.

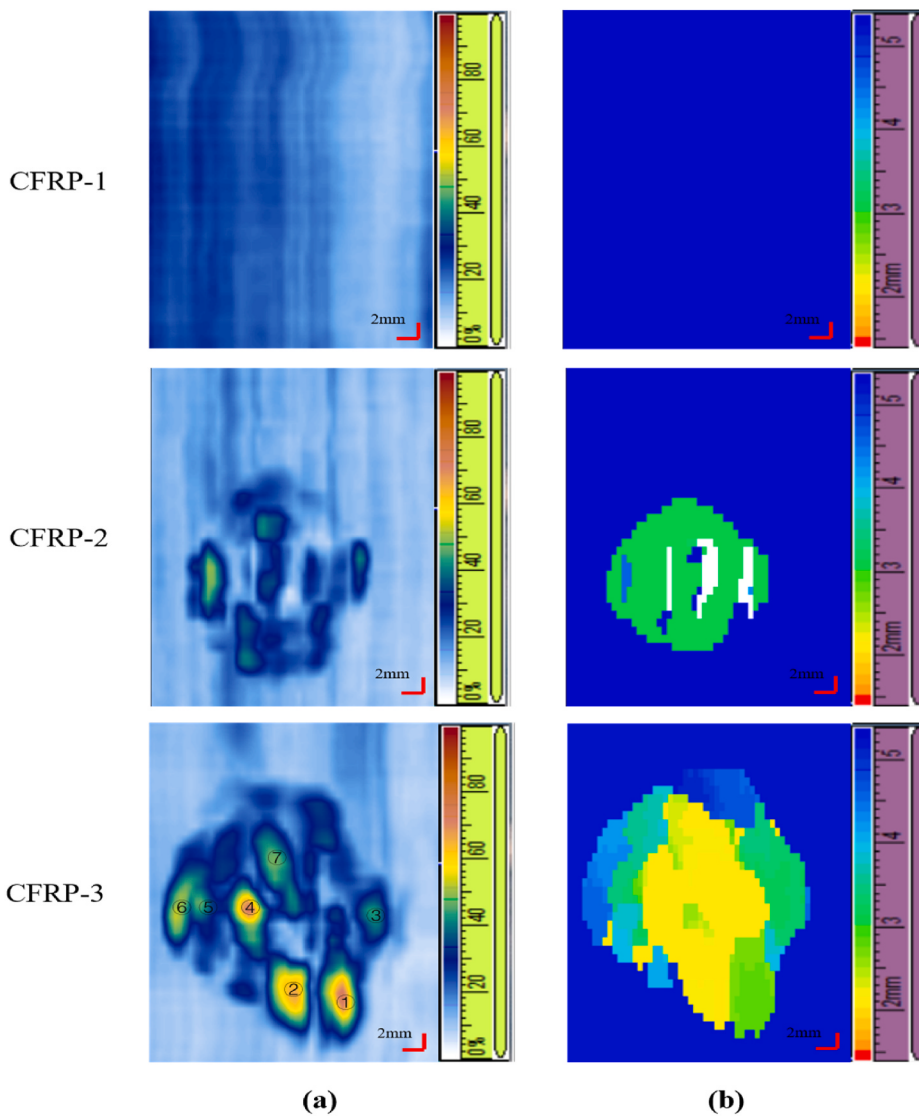


Fig. 7. Ultrasonic testing of CFRPs after the LVI test: a). C-scan; b). D-scan.

Table 2
Neural network data sets.

	Signal used (Train)	Signal used (Validation)	Signal used (Test)	Total
Marks	1887	564	243	2694

of LSTM is improved, so that the running time of CNN-LSTM is 23 s. With the help of the information from the neural memory unit, the accuracy of CNN-LSTM is higher than that of LSTM. The specific analysis would be given in the next section.

3.3. Classification identification and verification

To evaluate the performances of all the models on the ultrasonic data from the impacted sample, the dataset of the A-scan signals from the seven typical delamination damage in Fig. 7a was used to validate the trained networks. The estimation results are listed in Table 4, where the depth information gathered by D-scan data is also provided for reference.

After the ultrasonic scanning process, the CFRP-3 was cut by the wire cutting to investigate the delamination status. Three paths (A-A, B-B and

C-C in Fig. 8a) were chosen for the cutting line and the sectional images were captured by the optical microscope. As illustrated in Fig. 9b, the true depths of the delamination areas corresponding to the seven labeled reflection areas are measured and listed in Table 5.

4. Analysis and discussion

To further characterize the difference between the predicted results of each model and the true depth. The absolute value of the error of each damage depth relative to the true depth error was calculated based on the data from Tables 3 and 4, the ratio of the resulting depth difference to the true depth of the damage was the relative error, and the error results were illustrated in Fig. 10. The average depth relative errors of D-scan, LSTM, CNN and CNN-LSTM were 104.96%, 39.64%, 38.16% and 8.96%, respectively. The error of the D-scan was the largest and that of CNN-LSTM was the smallest.

The D-scan error was mainly influenced by a combination of three aspects: the anisotropic of carbon fiber composites [26], the reduction in signal echo amplitude due to ultrasonic attenuation [3], and the partial echo information of near-surface defects coupled in the first echo [2]. Neural network models (LSTM, CNN and CNN-LSTM) could effectively reduce the detection error of D-scan.

In the training process, the LSTM model utilized the gate unit of its

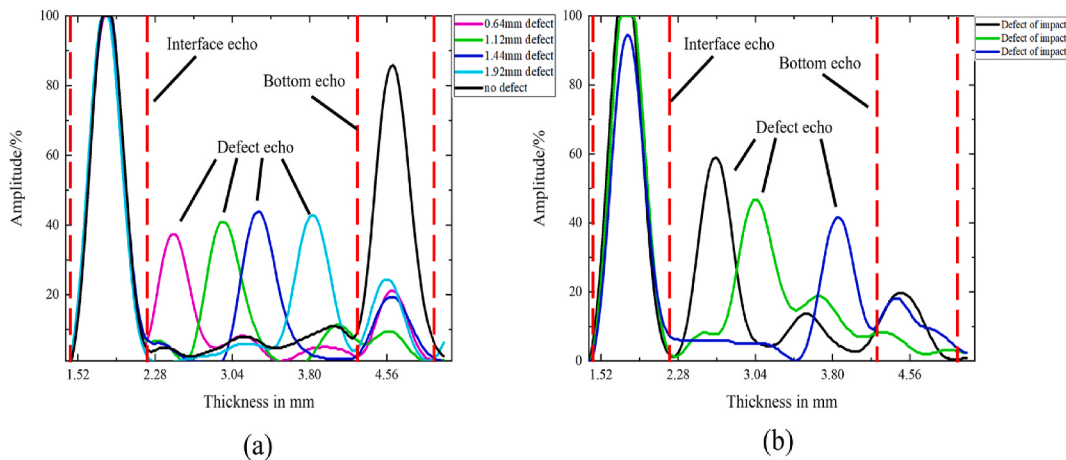


Fig. 8. Ultrasonic wave signal: a), ultrasonic signals of different artificial defects; b), ultrasonic signals of different impact defects.

Table 3
Evaluation index of different model.

Model	ACC	PRE	REC	F1
LSTM	0.9219	0.9002	0.9305	0.9151
CNN	0.9851	0.9782	0.9952	0.9883
CNN-LSTM	0.9628	0.9522	0.9649	0.9582

Table 4
Defect depth identification results and D-scan data.

Delamination ID	D-scan	LSTM	CNN	CNN-LSTM
1	1.72 mm	1.16 mm	1.16 mm	1.32 mm
2	1.31 mm	0.52 mm	0.52 mm	0.68 mm
3	2.30 mm	1.48 mm	1.64 mm	1.32 mm
4	1.23 mm	0.52 mm	1.00 mm	0.36 mm
5	2.56 mm	2.92 mm	1.8 mm	1.64 mm
6	3.63 mm	2.28 mm	2.92 mm	2.92 mm
7	1.35 mm	0.84 mm	0.36 mm	0.36 mm

memory neuron and nonlinear loss function (sigmoid) to determine the state of its memory nerve and update the weights of the internal gating [26], to give play to the temporal memory advantage of the neuron on the important feature information of the data [23], and the remaining information is selectively discarded by the gating unit. However, the complex gate operation of the memory neuron increased the computational volume and computing time of the model, which was less effective compared to CNN. In the CNN model, the convolutional neuron extracts the data features and selectively transmits the feature data to the local connectivity of the next connection unit [27] and shares them with each neuron parameter, that is, convolutional neurons use the same parameters to extract features [28] to reduce the number of parameters and thus accelerate the training speed [29]. Moreover, the convolutional

Table 5
The true depth of the labeled delamination areas.

Delamination ID	1	2	3	4	5	6	7
Depth (mm)	1.36	0.62	1.20	0.37	1.96	3.21	0.41

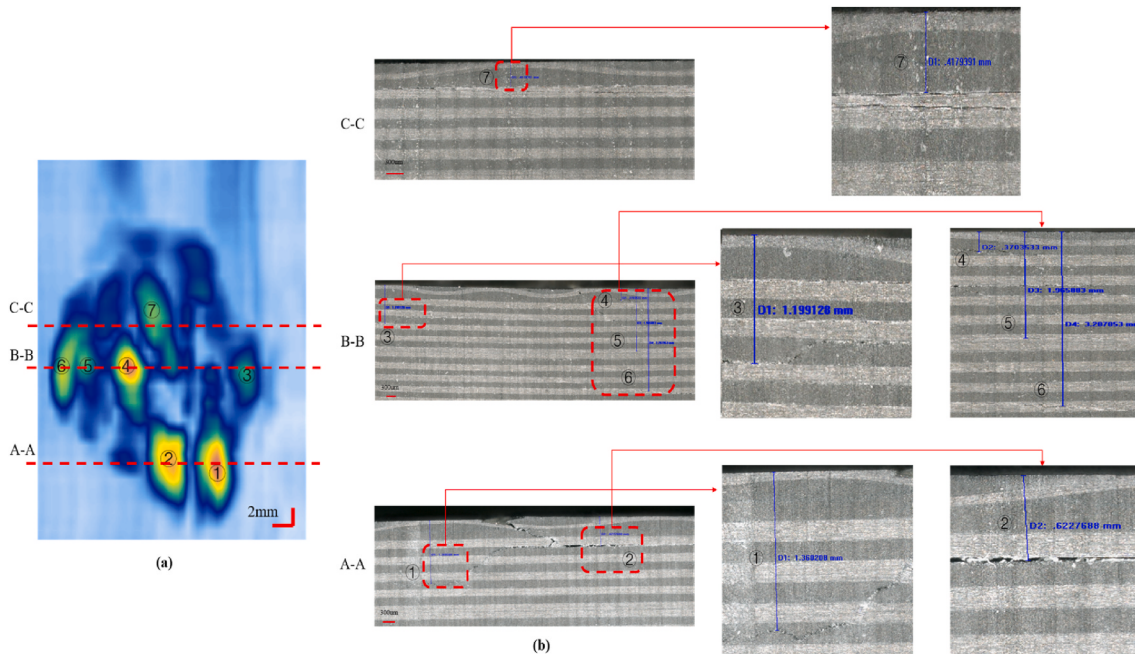


Fig. 9. The cutting paths along the labeled reflection regions and sectional images of the corresponding delamination damage.

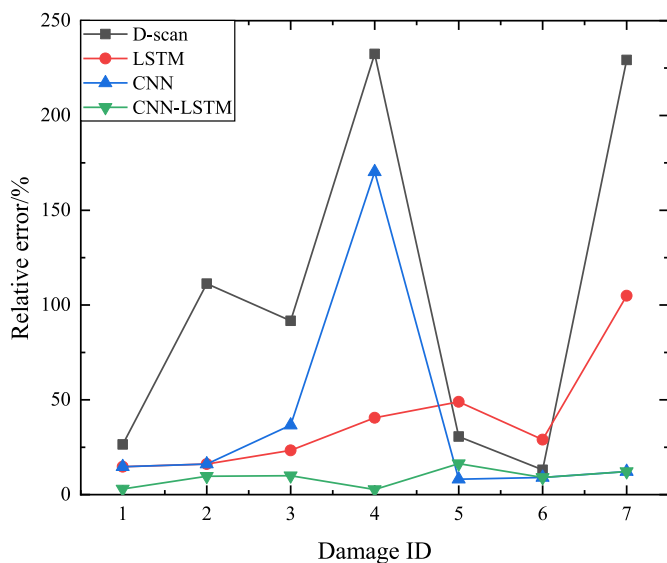


Fig. 10. The relative errors of four damage depth estimation methods.

layer was applied to extract the features of the time series [30], as well as the pooling layer to further extract the data features and reduce the dimensionality [31]. In the process of cross feature extraction by multiple convolutional neurons, the process lost a lot of valuable feature information [32], which included the correlation between whole objects and their parts [33]. This might be the reason why the model has high accuracy in the training phase but does not perform as well as CNN-LSTM on the impacting test set. CNN-LSTM further reduced the average error than the other two models with the combination of the advantages of feature extraction from CNN [34] and temporal memory from LSTM [23]. As illustrated in Fig. 10, the average errors of CNN-LSTM were all under D-scan and this model also performed better than the other models in most cases.

5. Conclusion

In this study, deep learning models were used to identify damage of unknown depth in CFRP, and the dataset of the model consists of ultrasonic A-scan signals of artificially defective CFRP. Based on the identification of the A-scan signals, the depth of unknown damage generated by the LVI test was then localized. To validate the trained networks, the impacted sample was cut off and the true depths of the damage were measured using an optical microscope. The depth information was used to verify the accuracies of the different deep learning models. The results shown that the hybrid deep learning model CNN-LSTM could effectively reduce the depth error of ultrasonic detection damage by employing the data feature extraction ability of CNN and the time memory advantage of LSTM, and the average depth relative error could be reduced to 8%.

In the future, polymer sheets would be used to create artificial defects inside the laminates, which should further increase the classification accuracy of the deep learning method.

CRediT authorship contribution statement

Xiaoying Cheng: Conceptualization, Methodology, Writing - Original Draft & Editing, Funding Acquisition.

Gaoshen Ma: Methodology, Data Analysis, Writing - Original Draft.

Zhenyu Wu: Conceptualization, Writing - Review & Editing, Funding Acquisition.

Hongfei Zu: Methodology, Writing - Review & Editing, Funding Acquisition.

Xudong Hu: Supervision, Writing - Review & Editing.

Declaration of competing interest

The authors declare that they have no known competing financial interests or personal relationships that could have appeared to influence the work reported in this paper.

Data availability

Data will be made available on request.

Acknowledgement

This work was financially sponsored by the National Natural Science Foundation of China (Grant Number 52175523 and U22A20182), “Pioneer” and “Leading Goose” R&D Program of Zhejiang (Grant Number 2022C01237), and Zhejiang Provincial Natural Science Foundation of China (Grant Number LGG20E050015 and LQ20E050020). All these supports are gratefully acknowledged.

References

- [1] Rani M, et al. A review on recycling and reuse methods for carbon fiber/glass fiber composites waste from wind turbine blades. Compos B Eng 2021;215:108768.
- [2] Blandford BM, Jack DA. High resolution depth and area measurements of low velocity impact damage in carbon fiber laminates via an ultrasonic technique. Compos B Eng 2020;188.
- [3] Wronkowicz A, Dragan K, Lis K. Assessment of uncertainty in damage evaluation by ultrasonic testing of composite structures. Compos Struct 2018;203:71–84.
- [4] Qu Z, Jiang P, Zhang W. Development and application of infrared thermography non-destructive testing techniques. Sensors 2020;20(14):3851.
- [5] Shoukroun D, et al. Enhanced composite plate impact damage detection and characterisation using X-Ray refraction and scattering contrast combined with ultrasonic imaging. Compos B Eng 2020;181.
- [6] Marcet A, Thomas JH, El Guerjouma R. Damage characterization of polymer-based composite materials: multivariable analysis and wavelet transform for clustering acoustic emission data. Mech Syst Signal Process 2008;22(6):1441–64.
- [7] Caminero MA, et al. Internal damage evaluation of composite structures using phased array ultrasonic technique: impact damage assessment in CFRP and 3D printed reinforced composites. Compos B Eng 2019;165:131–42.
- [8] Aymerich F, Meili S. Ultrasonic evaluation of matrix damage in impacted composite laminates. Compos B Eng 2000;31(1):1–6.
- [9] Morokov E, et al. High resolution ply-by-ply ultrasound imaging of impact damage in thick CFRP laminates by high-frequency acoustic microscopy. Compos Struct 2021;256:113102.
- [10] Hauffe A, Hähnle F, Wolf K. Comparison of algorithms to quantify the damaged area in CFRP ultrasonic scans. Compos Struct 2020;235:111791.
- [11] Sadeghi MZ, et al. Damage detection by double-sided ultrasonic assessment in low-velocity impacted CFRP plates. Compos Struct 2019;208:646–55.
- [12] Yang X, Ju B-F, Kersemans M. Assessment of the 3D ply-by-ply fiber structure in impacted CFRP by means of planar Ultrasound Computed Tomography (pU-CT). Compos Struct 2022;279:114745.
- [13] Wang X, et al. Three-dimensional damage quantification of low velocity impact damage in thin composite plates using phased-array ultrasound. Ultrasonics 2021; 110:106264.
- [14] Wronkowicz-Katunin A, Katunin A, Dragan K. Reconstruction of barely visible impact damage in composite structures based on non-destructive evaluation results. Sensors 2019;19(21).
- [15] Zhao X, et al. Active health monitoring of an aircraft wing with embedded piezoelectric sensor/actuator network: I. Defect detection, localization and growth monitoring. Smart Mater Struct 2007;16(4):1208.
- [16] Meng M, et al. Ultrasonic signal classification and imaging system for composite materials via deep convolutional neural networks. Neurocomputing 2017;257: 128–35.
- [17] Miorelli R, et al. Defect sizing in guided wave imaging structural health monitoring using convolutional neural networks. NDT E Int 2021;122:102480.
- [18] Cui R, et al. Damage imaging in skin-stringer composite aircraft panel by ultrasonic-guided waves using deep learning with convolutional neural network. Structural Health Monitoring; 2021.
- [19] Munir N, et al. Convolutional neural network for ultrasonic weldment flaw classification in noisy conditions. Ultrasonics 2019;94:74–81.
- [20] Guo Y, et al. Fully convolutional neural network with GRU for 3D braided composite material flaw detection. IEEE Access 2019;7:151180–8.
- [21] Gao F, et al. A softmax classifier for high-precision classification of ultrasonic similar signals. Ultrasonics 2021;112:106344.
- [22] Sasikumar A, et al. Impact and compression after impact response in thin laminates of spread-tow woven and non-crimp fabrics. Compos Struct 2019;215:432–45.
- [23] Shen Z, et al. Wind speed prediction of unmanned sailboat based on CNN and LSTM hybrid neural network. Ocean Eng 2022;254:111352.
- [24] Avanzato R, Beritelli F. Automatic ECG diagnosis using convolutional neural network. Electronics 2020;9(6):951.

- [25] Choung J, et al. Automatic discontinuity classification of wind-turbine blades using A-scan-based convolutional neural network. *Journal of Modern Power Systems and Clean Energy* 2021;9(1):210–8.
- [26] Graves A, Schmidhuber J. Framewise phoneme classification with bidirectional LSTM and other neural network architectures. *Neural Network* 2005;18(5–6): 602–10.
- [27] Wang DL. A comparison of CNN and LEGION networks. In: *Neural networks, 2004. Proceedings. 2004 IEEE international joint conference on*; 2004.
- [28] Savarese P, Maire M. Learning implicitly recurrent CNNs through parameter sharing. 2019.
- [29] Zhao R, et al. Deep learning and its applications to machine health monitoring. *Mech Syst Signal Process* 2019;115:213–37.
- [30] Nguyen THT, Phan QB. Hourly day ahead wind speed forecasting based on a hybrid model of EEMD, CNN-Bi-LSTM embedded with GA optimization. *Energy Rep* 2022; 8:53–60.
- [31] Bergmann P, et al. Uninformed students: student-teacher anomaly detection with discriminative latent embeddings. In: *IEEE conference on computer vision and pattern recognition (CVPR)*; 2020. June 2020.
- [32] Lin G, et al. RefineNet: multi-path refinement networks for dense prediction. *IEEE Transactions on Pattern Analysis and Machine Intelligence*; 2019. 1–1.
- [33] Shamsolmoali P, et al. Image super resolution by dilated dense progressive network. *Image Vis Comput* 2019;88:9–18.
- [34] Zhang S, Li CM, Ye W. Damage localization in plate-like structures using time-varying feature and one-dimensional convolutional neural network. *Mech Syst Signal Process* 2021;147:107107.